PCCP

Accepted Manuscript

ROYAL SOCIETY OF CHEMISTRY

www.rsc.org/pccp

Comparative Study of n-Dodecyl Tetraethylene Monoether Lytropic Liquid Crystals Incorporated with Graphene and Graphene Oxide

Lin Wang [a], Xia Xin [a, b *], Mengzhou Yang [a], Xin Ma [a], Zhenyu Feng [a], Rui Chen [a], Jinglin Shen [a], Shiling Yuan [a *]

[a] *Key Laboratory of Colloid and Interface Chemistry (Shandong University), Ministry of Education, Shanda nanlu No. 27, Jinan, 250100, P. R. China*

[b] *National Engineering Technology Research Center for Colloidal Materials, Shandong University, Shanda nanlu No. 27, Jinan, 250100, P. R. China*

[*] Author to whom correspondence should be addressed, E-mail: xinx@sdu.edu.cn.

Phone: +86-531-88363597. Fax: +86-531-88361008

[*] Author to whom correspondence should be addressed, E-mail: shilingyuan@sdu.edu.cn.

Phone: +86-531-88365896. Fax: +86-531-88564750

Abstract

Two kinds of carbon materials，i.e., graphene and graphene oxide (GO), were successfully incorporated into a lyotropic liquid crystal (LLC) matrix formed by n-dodecyl tetraethylene monoether ($C_{12}E_4$). The properties of graphene/$C_{12}E_4$ and GO/$C_{12}E_4$ LLC composites were characterized by UV-vis absorption, transmission electron microscopy (TEM) observations, polarized optical microscopy (POM) observations, small-angle X-ray scattering (SAXS) and rheological measurements. SAXS results indicate that both graphene and GO are well-dispersed in the $C_{12}E_4$ LLC matrix and some interactions occur between $C_{12}E_4$ LLC matrix and graphene (or GO) sheets. Moreover, it is demonstrated that graphene interacts with the hydrophobic part of $C_{12}E_4$ LLC while GO mainly interacts with the hydrophilic part of $C_{12}E_4$ LLC because of the different properties of graphene and GO. Integration of graphene and GO into $C_{12}E_4$/PEG systems by a spontaneous phase separation method reveals the different interaction mechanisms of graphene and GO with $C_{12}E_4$ LLC. It can be concluded that the mechanical and electrical properties of the $C_{12}E_4$ LLC have been largely improved by the incorporation of graphene and GO, which opens the door for wide applications in nanotechnology, electrochemical and biochemical areas.

Keywords: Graphene, graphene oxide, liquid crystal, SAXS, rheological properties

Introduction

Carbon-based materials, ranging from activated carbons (ACs) and one-dimensional (1D) carbon nanotubes (CNTs) to two-dimensional (2D) graphene nanosheets [1-3], hold great technological promise for a variety of sustainable energy applications. Carbon materials possess various desirable advantages, such as low-cost, light weight, adjustable porosity, varieties of forms, ease of processability, and controllable heteroatom doping [4-7]. Graphene, a single-layer and two-dimensional carbon lattice, was first reported in 2004 [8] and has been widely investigated because of its unique mechanical, quantum and electrical properties [9-12]. Graphene oxide (GO), a modified form of graphene, consists of a two-dimensional (2D) sheet of covalently bonded carbon atoms bearing various oxygen functional groups (e.g. hydroxyl, epoxide, and carbonyl groups) on their basal planes and edges. Therefore, GO is hydrophilic and can be readily dispersed in water as individual sheets to form stable colloidal suspensions [13-15]. Meanwhile, the oxygen-containing groups also impart new functions to GO, one of which is the interaction with small polar molecules such as surfactants and polymers to form GO intercalated or exfoliated composites [16, 17].

Organizing materials at small length scales is of great importance for the control of their properties. Liquid crystals (LC), including thermotropic liquid crystals and lytropic liquid crystals (LLC), are fluid but at the same time are long-range ordered. They represent a novel type of templates for realizing ordered functional composites [18]. LC has been successfully used to induce the alignment of dispersed carbon nanotubes (CNTs) [19-25]. Jiang et al. constructed a hexagonal columnar lyotropic phase with a nonionic polyoxy-ethylene surfactant ($C_{16}EO_6$) and an ionic liquid (EAN), which was then used for dispersing multi-walled carbon nanotubes (MWNTs) [19]. They also exploited the lubricating properties of the CNT–LC composites [19]. Lynch et al. found that

single-walled carbon nanotubes (SWNTs) and MWNTs can be aligned in nematic LCs formed by 4′-pentyl-4-cyanobiphenyl (5CB), and E7 (a mixture of alkyl- and alkoxycyanobiphenyls), respectively [20]. Weiss et al. worked with water-based systems. They used the nonionic surfactant Triton X-100 to construct the hexagonal columnar LLC and dispersed SWNTs either in Triton X-100 or in SDS. An enlarged spacing of the hexagonal columnar structure and an increased viscosity upon SWNTs introduction was detected by X-ray diffraction and rheological measurements, respectively [26]. In our previous work, we also successfully incorporated CNTs into nonionic polyoxy-ethylene surfactants ($C_{12}E_4$ and $C_{12}E_6$) LLC matrix at room temperature through spontaneous phase separation induced by hydrophilic polymer, i.e., poly (ethylene glycol) (PEG) [27-29].

In this paper, we give a detailed study of the incorporation of graphene and graphene oxide into n-dodecyl tetraethylene monoether ($C_{12}E_4$) LLC. The performance of graphene/$C_{12}E_4$ and graphene oxide/$C_{12}E_4$ composites were characterized by visual inspection, UV-vis-NIR measurements, transmission electron microscopy (TEM) observations, polarized optical microscopy (POM) observations, small-angle X-ray scattering (SAXS) and rheological measurements. The factors including the structures and concentrations of graphene (or graphene oxide) which can influence the characteristics of the composites, have been fully evaluated.

Experimental Section

Chemicals and Materials

N-dodecyl tetraethylene monoether ($C_{12}E_4$) with a purity of > 99% was purchased from Acros Organics (USA). Graphene (diameter: 0.5~2 μm; thickness: ~0.8 nm) and graphene oxide (diameter: 0.5~5 μm; thickness: 0.8~1.2 nm) were obtained from Nanjing XFNANO Materials Tech Co., Ltd.

PEG with molecular weight of 20000 g mol^{-1} was purchased from Sinopharm Chemical Reagent Company. All the above reagents were used without further purification. Water used in the experiments was triply distilled by a quartz water purification system.

Methods and Characterization

The phase diagram of $C_{12}E_4$ indicates the formation of a lamellar phase between 25 and 75 wt % at a temperature range of 298-323 K [30].

For graphene dispersions, a stock solution of 0.2 wt % $C_{12}E_4$ was prepared by dissolving the desired amount of $C_{12}E_4$ in water at room temperature. Dispersions of graphene in 0.2 wt % $C_{12}E_4$ aqueous solution were obtained by sonicating the mixtures for 45 min at 40 kHz and 250 W using a KQ-250DB ultrasonic apparatus (Shanghai). Then, a homogeneous black dispersion was obtained, which contains well-dispersed graphene as well as large aggregates. A small amount of black precipitates were noticed after deposition at room temperature for 2 weeks. The upper phase, which can be stable at room temperature for months, was collected for further use. For graphene oxide dispersions, a suspension of graphene oxide sheets was obtained under ultrasonication for 3 h in deionized water.

Aqueous dispersions of graphene (or graphene oxide) at different concentrations were added to the preformed LCs with a total concentration of $C_{12}E_4$ to be 35 wt %. After that, the samples were warmed to 333 K for better mixing.

UV-vis-NIR measurements were carried out on a computer-manipulated spectrometer (UV-vis 4100, Hitashi, Japan). TEM observations were carried out on a JEOL JEM-100 CXII (Japan) at an accelerating voltage of 80 kV. Polarized optical microscopy observations were performed by an AXIOSKOP 40/40 FL (ZEISS, Germany) microscope. Samples were prepared by directly dropping

several drops of samples into a 1 mm thick trough.

The obtained LC phases were characterized by an HMBG-SAX small angle X-ray scattering system (Austria) with a Ni-filtered Cu Kα radiation (0.154 nm) operating at 50 kV and 40 mA. The distance between the sample and detector was 27.8 cm.

The rheological measurements were carried out on an Anton Paar Physica MCR302 rheometer with a cone-plate system (diameter, 25 mm; cone angle, 2°). For the shear-dependent behavior, the viscosity measurements were carried out at shear rates ranging from 1 to 1000 s^{-1}. In oscillatory measurements, an amplitude sweep at a fixed frequency of 1 Hz was performed prior to the following frequency sweep in order to ensure that the selected stress was in the linear viscoelastic region. The viscoelastic properties of the samples were determined by oscillatory measurements in the frequency range of 0.01-10 Hz. The samples were measured at 20.0 ± 0.1 °C with the help of a cyclic water bath.

Results and Discussion

Dispersion States of Graphene and Graphene Oxide

A series of samples with 5 mL 0.2 wt % $C_{12}E_4$ and increasing amount of graphene are shown in Figure 1 and the effect of the amount of initially added graphene on graphene/$C_{12}E_4$ dispersions was investigated by visual inspection and UV-vis-NIR measurements (Figure 2A). It was found that the absorbance did not increase continuously with increasing amount of initially added graphene. Instead, it passed through a maximum at 0.3 mg mL^{-1} and then decreased (Figure 2B), which is consistent with the visual observations. Thus, the dispersion containing 0.2 wt % $C_{12}E_4$ and 0.3 mg mL^{-1} (i.e., sample C in Figure 1) was selected for further study.

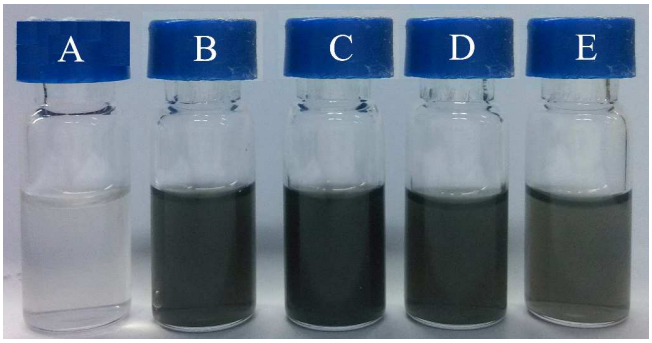

Figure 1 Photos of the supernatant of dispersions of graphene in 5 mL of 0.2 wt % $C_{12}E_4$ aqueous solutions. The samples were stored for more than one month before the supernatant were taken out for photos and the precipitated graphene at the bottom has been discarded. The amount of initially added graphene is 0.5 (A), 1.0 (B), 1.5 (C), 2.0 (D) and 2.5 mg (D), respectively. Each of the supernatant was diluted for ten times for better comparison.

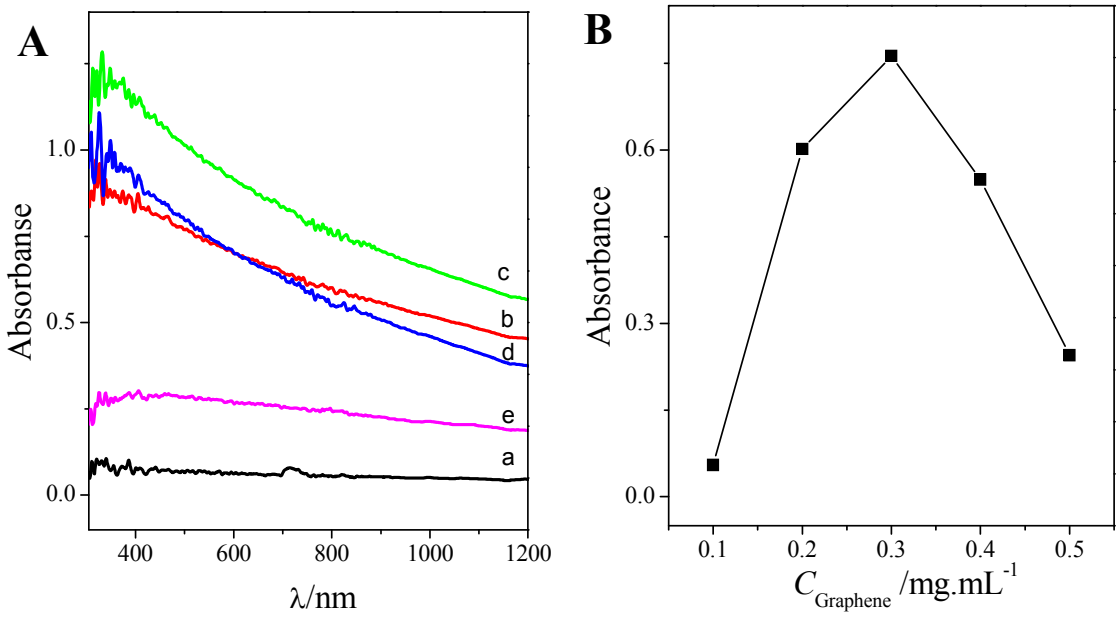

Figure 2 (A) UV-vis-NIR absorptions in the 300-1200 nm region for the supernatants of graphene dispersions. Curves a-e corresponding to sample A-E in Figure 1. (B) Change of absorbance at 800 nm as a function of initially added graphene.

Graphene oxide can be dispersed in water directly by ultrasonication at the level of individual

sheets and the dispersions can be stable for months. This can be ascribed to the presence of the oxygen-containing functional groups such as -COOH and -OH on the surfaces of GO. When dispersed in water, the carboxyl and phenolic hydroxyl groups on the GO sheets can be ionized. This will introduce electrostatic repulsion between adjacent GO sheets, accounting for the long-term stabilization of the GO dispersions [31].

Typical TEM images of dispersions of 0.3 mg mL^{-1} graphene in 0.2 wt% $C_{12}E_4$ aqueous solution and GO in water are given in Figure 3A and 3B, respectively. In the both cases, the graphene or GO sheets are plicated with low contrast, which is characteristic of individual sheets [37]. It indicates that both graphene and GO have been fully exfoliated and well-dispersed in aqueous solutions.

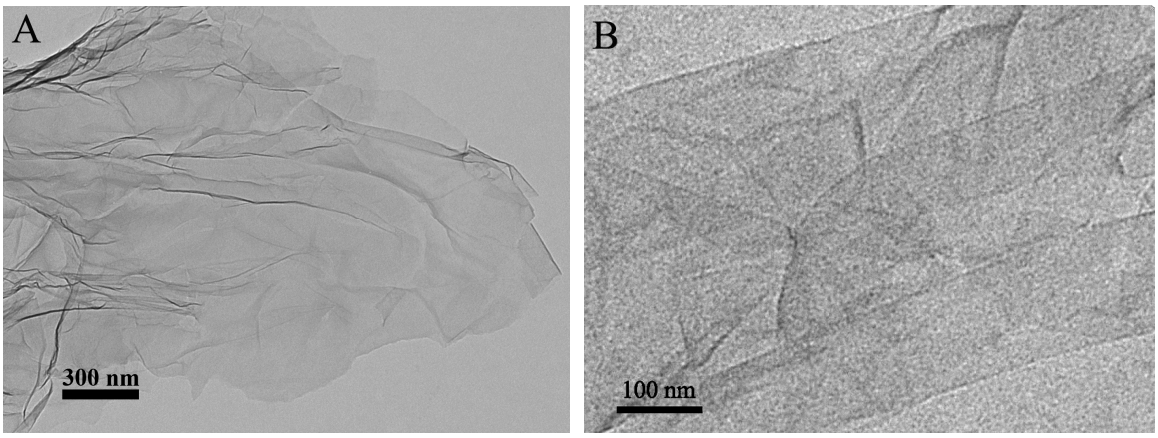

Figure 3 TEM images of A) sample C shown in Figure 1 and B) graphene oxide dispersed in water.

Formation of graphene/$C_{12}E_4$ and graphene oxide/$C_{12}E_4$ LLC composites

After mixing different concentrations of the dispersions of graphene (or graphene oxide) with $C_{12}E_4$ LLC, graphene/$C_{12}E_4$ (Figure 4A) and graphene oxide/$C_{12}E_4$ (Figure 4B) LLC composites were formed. No phase separation occurs, indicating the composites are stable and both graphene and graphene oxide are well dispersed in the $C_{12}E_4$ LLC matrix. The good stability of the LLC composites is also indicative of possible interactions existing between $C_{12}E_4$ LLC matrix and

graphene (or graphene oxide) sheets. Under polarized optical microscope, all of the composites show maltese crosses (Figure 5), which are characteristic of lamellar structures [29]. For graphene/$C_{12}E_4$ LLC composites, the contrast of the micrograph and the maltese crosses texture decreased with increased concentration of graphene, as can be seen in Figure 5B and 5C. This indicates that the incorporation of graphene might cause some changes of the host $C_{12}E_4$ LLC matrix. At high concentrations of graphene, small aggregates of graphene may also exist in the matrix. These assumptions are further confirmed by small angle X-ray scattering (SAXS) study as shown below.

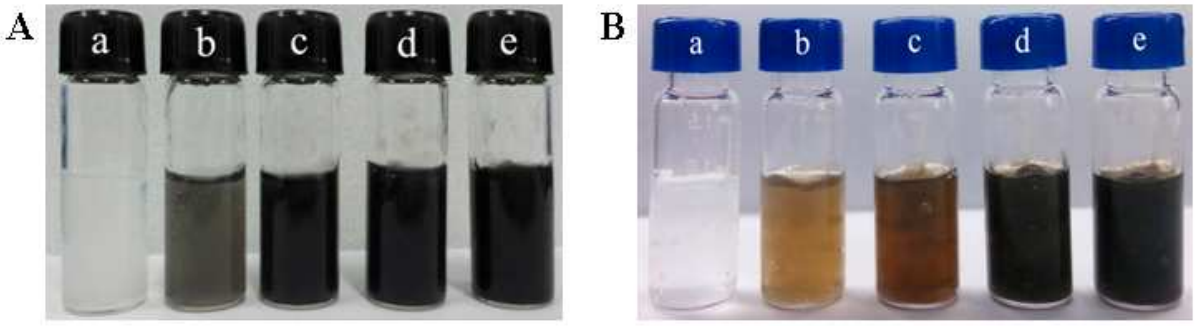

Figure 4 Graphene (A) and graphene oxide (B) incorporated into LLC phase formed by 35 wt % $C_{12}E_4$. The weight percent of graphene and GO is 0 (a), 0.03 (b), 0.09 (c), 0.15 (d), 0.20 (e) mg.mL^{-1} in (A) and 0 (a), 0.1 (b), 0.5 (c), 1.0 (d) 1.5 (e) mg.mL^{-1} in (B), respectively.

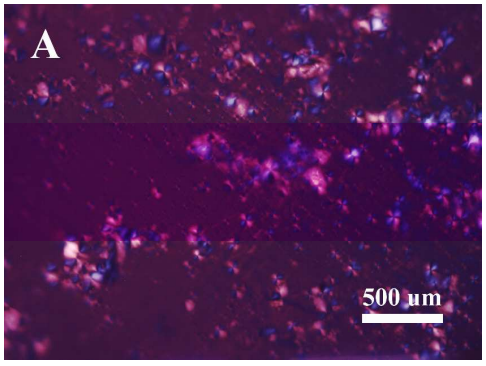

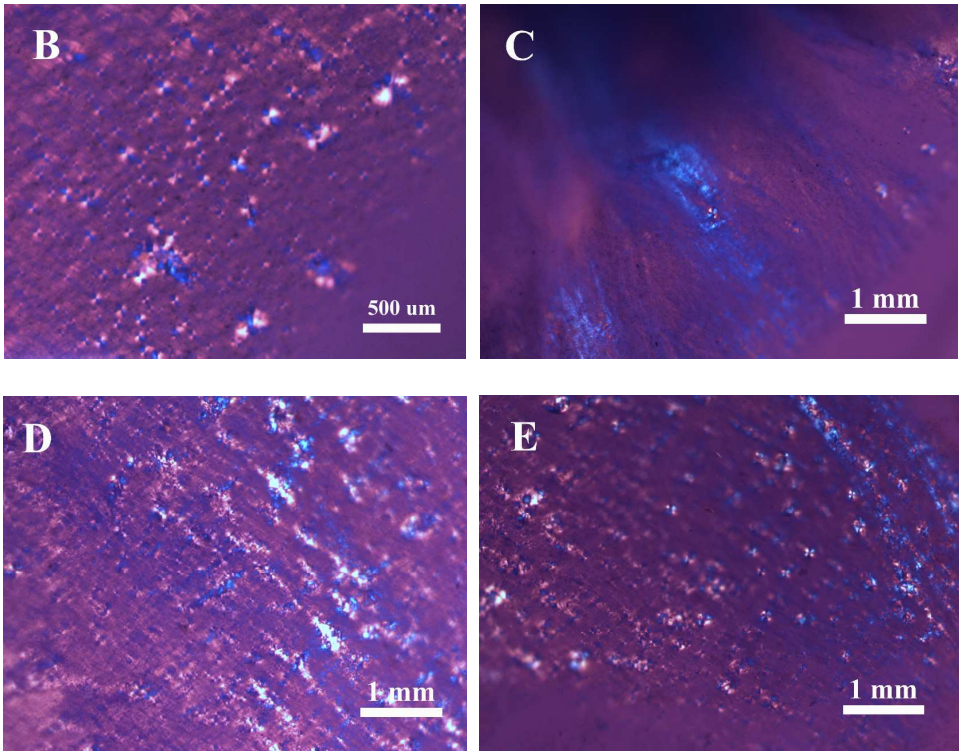

Figure 5 POM images for graphene/$C_{12}E_4$ (A-C) and GO/$C_{12}E_4$ (D, E) LLC composites. The concentration of $C_{12}E_4$ is fixed at 35 wt % while that of graphene or GO is 0 (A), 0.15 (B), 0.2 (C), 0.5 (D) and 1.0 (E) mg mL^{-1}, respectively.

SAXS Measurements

To gain further details about graphene/$C_{12}E_4$ and GO/$C_{12}E_4$ LLC composites, SAXS measurements were carried out as a function of the concentration of graphene and graphene oxide. Two peaks were detected with a relative position ratio of 1:2 (Figure 6A), as expected for the (100) and (110) reflections of the lamellar phase [32, 33]. From the q value of the first peak, the inter-lamellar distance, denoted as d-spacing, can be calculated ($d = 2\pi/q_{max}$). For graphene/$C_{12}E_4$ LLC composites the d-spacing increased continuously at low-to-medium concentration of graphene (Figure 6B). For example, the d-spacing at the presence of 0.03 wt % graphene is 9.81 nm. It shifts to 10.25 nm when the concentration of graphene changes to 0.09 wt %. A schematic illustration of the interaction between graphene and $C_{12}E_4$ LLC phase is given in Scheme 1, which shows that the

incorporation of graphene sheets into the hydrophobic part of $C_{12}E_4$ LLC phase enlarges the hydrophobic region of the LLC phase and increases *d*-spacing. When the concentration of the incorporated graphene is higher than 0.09 wt %, however, a decrease in *d*-spacing was noticed (from 10.25 nm to 9.80 nm). This is probably due to the microscopic phase separation of graphene within the LLC matrix, which is further proved by rheological measurements (see below). Moreover, these observations were also consistent with our previous results about the interaction between CNTs and $C_{12}E_4$ LLC phase [30]. This indicates that both graphene and CNTs behave similarly in LLC matrix, although they have different dimensionalities (i.e., two-dimensional vs. one-dimensional).

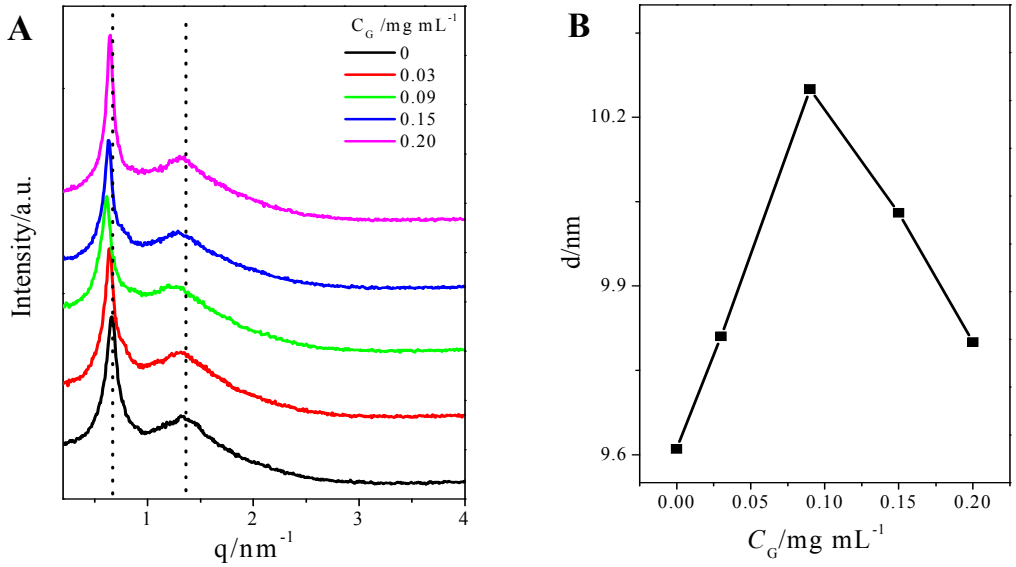

Figure 6 SAXS results (A) and variation of *d*-spacing (B) of graphene/35 wt % $C_{12}E_4$ LLC composites as a function of the concentration of graphene.

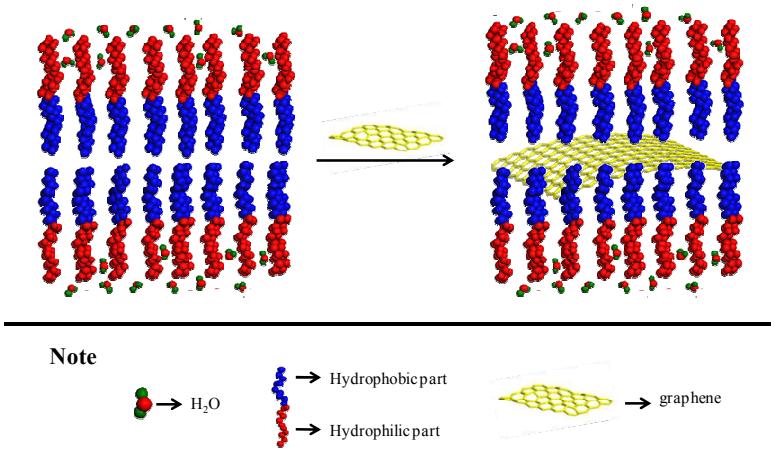

Scheme 1 Schematic illustrations of the interaction between graphene and $C_{12}E_4$ LLC phase. Graphene is expected to locate in the hydrophobic part of the LLC matrix.

For GO/$C_{12}E_4$ LLC composites, when the concentration of GO changed from 0.1 wt % to 1.5 wt % while the concentration of $C_{12}E_4$ was fixed at 35 wt %, the composites were always lamellar phase (Figure 7A) and the addition of GO induces a continuously decrease of *d*-spacing (Figure 7B). A schematic illustration of the interaction between GO and $C_{12}E_4$ LLC phase is given in Scheme 2. Generally speaking, when the material is doped into LLC phase, it usually induces the increase of *d*-spacing. When GO was doped as in current case, however, it induces a decrease of *d*-spacing. We tentatively ascribe this phenomenon to the following reasons: 1) Each GO sheet only has one carbon atom thickness, thus it has little effect on the *d*-spacing of LLC phase; 2) There are a lot of hydrophilic groups modified on each GO sheet, which induces a large number of hydrogen bonds between GO and water. This will restrict the movement of water molecules and compress the hydrophilic layer of the LLC phase; 3) The hydrophilic group on the GO sheet can also form a large number of hydrogen bonds with the EO chain of $C_{12}E_4$, which will induce the entanglement between GO and $C_{12}E_4$ and condenses the hydrophilic layer of $C_{12}E_4$ LLC phase.

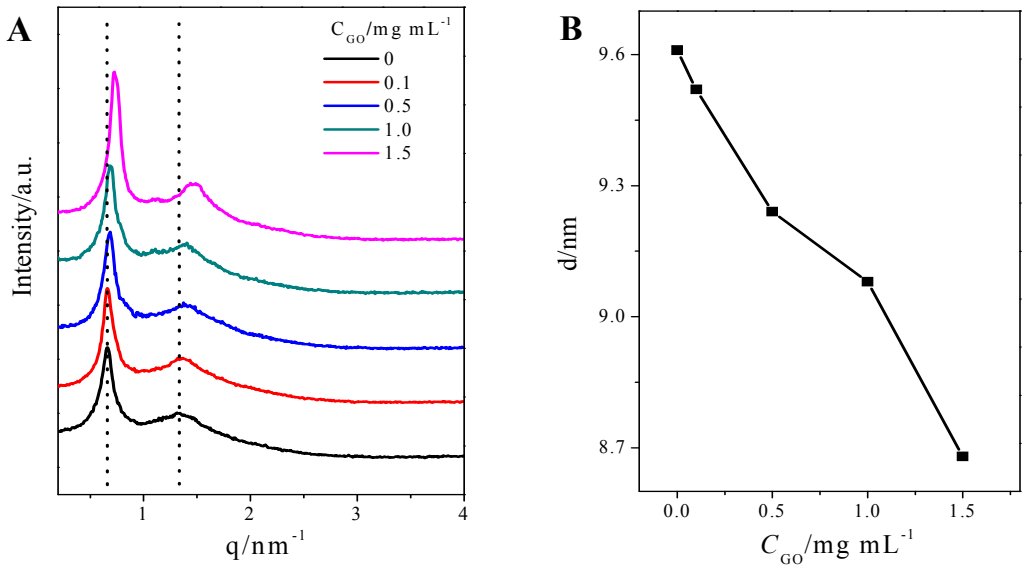

Figure 7 SAXS results (A) and variation of *d*-spacing (B) of GO/35 wt % $C_{12}E_4$ LLC composites as a function of the concentration of GO (C_{GO}).

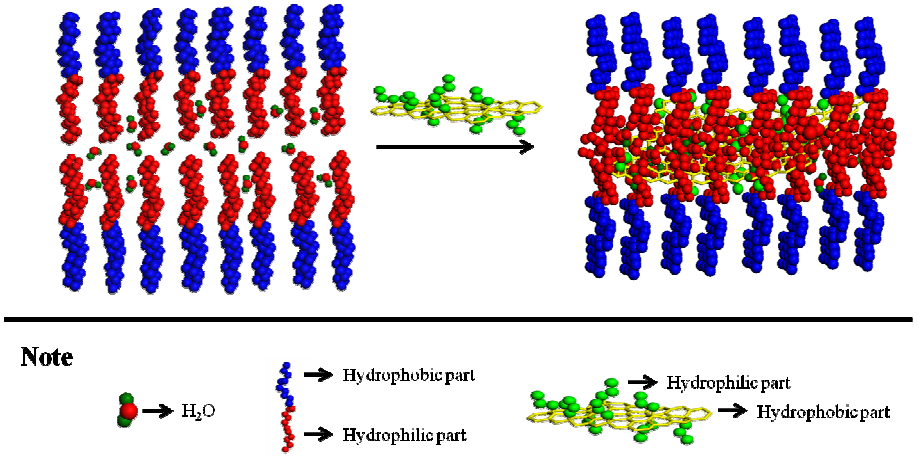

Scheme 2 Schematic illustrations of the interaction between GO and $C_{12}E_4$ LLC phase. GO is expected to locate in the hydrophilic part of the LLC matrix.

Rheological Properties

Rheology is a key method to investigate LLC, from which the viscoelastic properties of the system can be extracted. The high surface area of graphene and GO nanosheets can induce relatively high interfacial interactions in the LLC phase, which impart interesting dynamic

viscoelastic properties to the composites. The influences of graphene on the rheological properties of the $C_{12}E_4$ LLC were investigated and the results are given in Figure 8. The concentration of $C_{12}E_4$ was fixed at 35 wt % while that of graphene was varied. When the stress sweep test was performed at a fixed frequency of 1.0 Hz (Figure 8A), a critical stress value (yield stress, denoted as τ^*) was detected beyond which composites start to flow. Generally, τ^* is used as a measure to evaluate the strength of a given network structure. From Figure 8A, it can be seen that τ^* of the graphene/ $C_{12}E_4$ LLC composites is ~ 4 Pa, indicating considerable mechanical stability of the composites. Beyond τ^*, the shear modulus sharply decreased and a Newtonian-like flow was observed due to the destruction of the graphene/$C_{12}E_4$ LLC network structure [34, 35].

Frequency sweep in Figure 8B shows that G' is higher than G″ over the studied frequency range, demonstrating the "solid-like" rheological property of the composites. Figure 8C denotes that η^* decreases with the increase of frequency, indicating a shear-thinning behavior. All of these are characteristic for LLC systems [36]. It can be seen that the strength of the graphene/LLC composite can be enhanced even only a small amount of graphene was added. With the increase of C_{Graphene} the elastic modulus of the composite increased gradually (Figure 8D). But adding excessive graphene decreases the strength of the composite. Thus, it turns out that $C_{12}E_4$ can create efficient steric repulsions between individual graphene sheets and enhance the strength of the composite at low-to-medium C_{Graphene}, while the stabilization by the steric effect of $C_{12}E_4$ is insufficient to well separate the graphene sheets at high C_{Graphene}. In the latter case, flocculation and aggregation of graphene sheets may occur, thereby destroying the long-range ordering of the LLC martix and ultimately decreases the strength of the composite [30]. These observations were similar to our previous results on CNTs/$C_{12}E_4$ LLC composites.

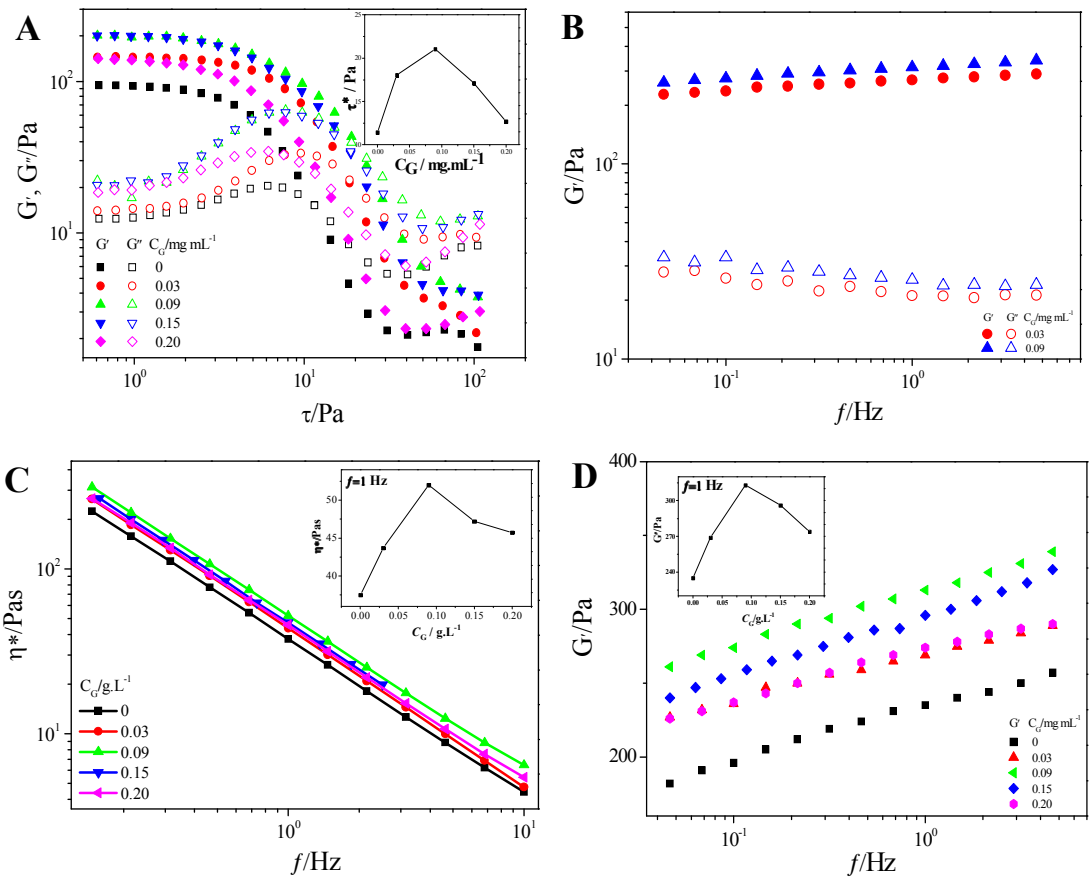

Figure 8 Rheological results for graphene/35 wt % $C_{12}E_4$ LLC composites at the presence of different concentration of graphene. (A) G′ and G″ as a function of the applied stress at a constant frequency (1.0 Hz). Variations of G′ and G″ (B), η* (C) and G′ (D) as a function of frequency. Inset of A, C and D are the variation of τ^*, η* and G′ as a function of C_{Graphene}.

For GO/$C_{12}E_4$ LLC composites, similar phenomenon was observed, i.e., in the stress sweep the network structure of the composite was destroyed when the stress exceeds τ^*, beyond which a Newtonian-like flow was noticed (Figure 9A). In frequency sweep, G′ is higher than G″ over the whole frequency range (Figure 9B) and η^* decreases with the increase of frequency (Figure 9C). However, different from the trend observed in graphene/$C_{12}E_4$ LLC system, G′ of the GO/$C_{12}E_4$ LLC composite increases continuously with increasing C_{GO} (Figure 9D), which reveals a continuous strengthened network structure. Thus the introduction of GO to $C_{12}E_4$ LLC matrix

monotonously improves the mechanical strength of the system. This could be due to the formation of hydrogen bonds between the oxygen-containing functional groups (–COOH and –OH) on the surfaces of GO and the −OH groups of $C_{12}E_4$. Current study indicates that GO can act as nanofillers to enhance the mechanical performance of the LC system, which is consistent with the conclusions obtained by others [37].

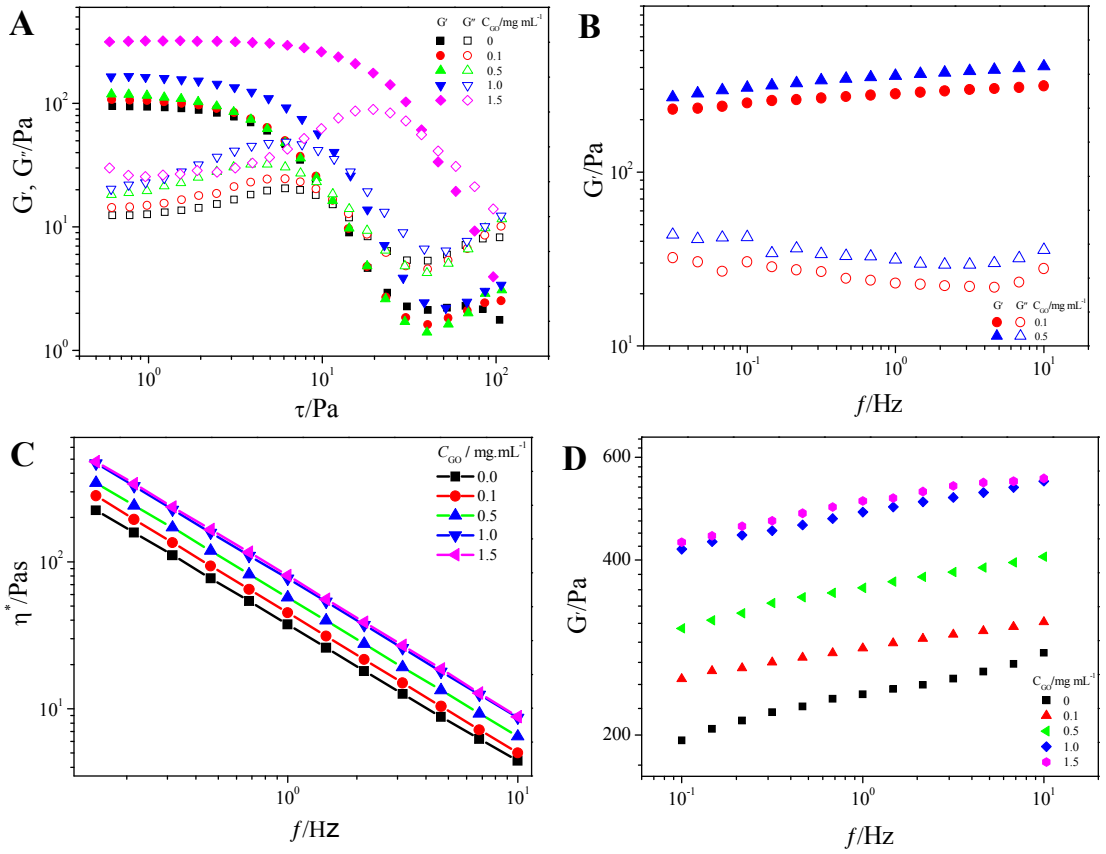

Figure 9 Rheological results for GO/35 wt % $C_{12}E_4$ LLC composites at the presence of different concentration of GO. (A) G′ and G″ as a function of the applied stress at a constant frequency (1.0 Hz). Variations of G′ and G″ (B), η* (C) and G′ (D) as a function of frequency.

Formation mechanism of graphene/$C_{12}E_4$ and graphene oxide/$C_{12}E_4$ LLC composites

To get insights of the different interaction mechanisms dominated in graphene/$C_{12}E_4$ LLC and GO/$C_{12}E_4$ LLC composites, a phase separation process was designed. Briefly, hydrophilic polymer

PEG with a molecular weight of 20000 (denoted as PEG 20000 hereafter) was added to graphene/$C_{12}E_4$ LLC and GO/ $C_{12}E_4$ LLC composites, respectively, and the phenomena during the phase separation were recorded. Because of the hydrophobic nature of graphene, it has no interaction with water and PEG 20000 molecules. Thus, during phase separation all graphene nanosheets entered the upper LLC phase without any precipitation (Figure 10A). This phenomenon is similar to our previous results on CNTs/LLC composites [28-30]. In case of GO, however, the nanosheets can interact with both PEG 20000 and $C_{12}E_4$ due to their amphiphilic properties induced by the presence of both hydrophilic groups and the hydrophobic carbon plane. When C_{GO} is low, most of the nanosheets interact with PEG 20000 and stay in the bottom phase (Figure 10B). Only a small amount of nanosheets were found in the upper phase ($C_{12}E_4$-rich phase) [28-30]. But when C_{GO} is high, strong interactions between PEG 20000 and graphene oxide were induced. In this case the water molecules were effectively captured and phase separation was prevented, leaving a homogeneous black phase as seen in Figure 10 B (d).

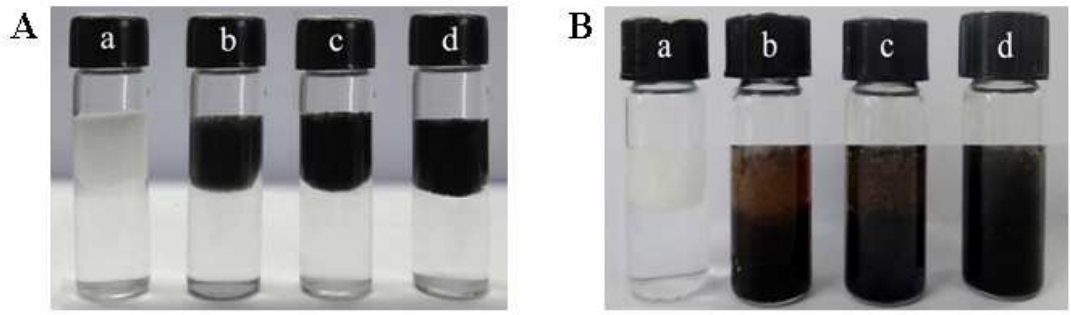

Figure 10 The states of graphene (A) and GO (B) embedded in 10 wt % $C_{12}E_4$ and 20 wt % PEG 20000 mixed systems. The weight percents of graphene and GO dispersion were 70 wt %. The weight percent of graphene and GO in the dispersions were 0 (a), 0.04 (b), 0.08 (c), 0.13 (d) mg·mL^{-1} in A and 0 (a), 1.7 (b), 2.6 (c), 5.2 (d) mg·mL^{-1} in B, respectively.

The states of graphene and GO nanosheets incorporated in $C_{12}E_4$ LLC matrix at both low and

high concentrations are illustrated in Scheme 3. For graphene/$C_{12}E_4$ LLC composites, we conclude based on our observations and experimental results that the nanosheets can be efficiently stabilized by the steric repulsions created by $C_{12}E_4$. The strength of the composite can be enhanced by the addition of a small amount of well-dispersed graphene and a maximum strength was obtained at a suitable $C_{Graphene}$. When the added graphene is excessive, however, the steric stabilizations induced by $C_{12}E_4$ are insufficient to well disperse the nanosheets. It causes the flocculation of the nanosheets and thereby destroys the long-range order of the LLC matrix, leading to a decrease of the strength of the composite. But for GO/$C_{12}E_4$ LLC composites, the oxygen-containing groups on the GO surface can interact effectively with $C_{12}E_4$ through hydrogen bonding. This greatly enhances the unidirectional dispersion of GO nanosheets in $C_{12}E_4$ matrix and improves the mechanical strength of the composite [31].

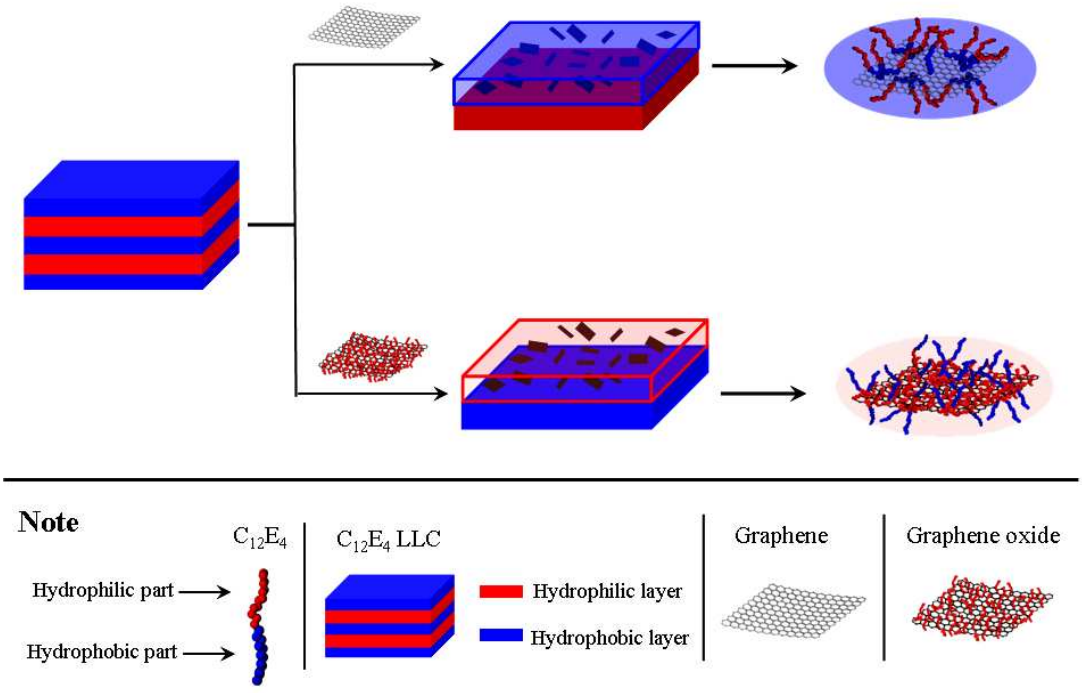

Scheme 3 Schematic illustration of graphene and GO incorporated into $C_{12}E_4$ LLC phase. Graphene incorporates into the hydrophobic layers of $C_{12}E_4$ LLC phase while GO tends to stay in the hydrophilic layers.

Conclusions

To conclude, graphene and GO have been successfully incorporated into the lamellar lyotropic liquid crystals formed by $C_{12}E_4$. From the experimental results, it can be seen that graphene has been fully exfoliated and well-dispersed in $C_{12}E_4$ aqueous solutions. Both graphene/$C_{12}E_4$ LLC and GO/$C_{12}E_4$ LLC composites preserve the typical texture of maltese crosses under POM, indicating that the addition of graphene and GO didn't markedly change the properties of $C_{12}E_4$ LLC. SAXS and rheological measurements indicate that graphene/$C_{12}E_4$ LLC and GO/$C_{12}E_4$ LLC composites have different properties because of the different nature of graphene and GO. In order to verify this phenomenon, we also used phase separation method to further confirm the different interaction mechanisms of graphene and GO with $C_{12}E_4$ LLC. At last, a mechanism for the formation of stable graphene/$C_{12}E_4$ LLC and GO/$C_{12}E_4$ LLC composites is proposed, i.e., graphene interacts with the hydrophilic part while GO interacts with the hydrophobic part of $C_{12}E_4$ LLC. Our results should facilitate the manipulation and processing of graphene and GO materials for various applications.

Acknowledgement

We gratefully acknowledge financial support from the Natural Science Foundation of China (21173128, 21203109) and Independent Innovation Foundation of Shandong University (IIFSDU, 2012GN015).

References

[1] C. G. Lee, X. D. Wei, J. W. Kysar and J. Hone, *Science*, 2008, **321**, 385-388.

[2] P. Avouris, Z. H. Chen and V. Perebeinos, *Nat. Nanotechnol.*, 2007, **2**, 605-615.

[3] N. A. Kotov, *Nature*, 2006, **442**, 254-255.

[4] A. K. Geim and K. S. Novoselov, *Nature Materials*, 2007, **6**, 183-191.

[5] X. M. Yang, Y. F. Tu, L. Li, S. M. Shang and X. M. Tao, *ACS Appl. Mater. Interfaces*, 2010, **2**, 1707-1713.

[6] X. Huang, X. Y. Qi, F. Boey and H. Zhang, *Chemical Society Reviews*, 2012, **41**, 666-686.

[7] J. C. Wang and S. Kaskel, *J. Mater. Chem.*, 2012, **22**, 23710-23725.

[8] K. S. Novoselov, A. K. Geim, S. V. Morozov, D. Jiang, Y. Zhang, S. V. Dubonos, I. V. Grigorieva and A. A. Firsov, *Science*, 2004, **306**, 666.

[9] K. S. Novoselov, A. K. Geim, S. V. Morozov, D. Jiang, M. I. Katsnelson, I. V. Grigorieva, S. V. Dubonos and A. A. Firsov, *Nature*, 2005, **438**, 197–200.

[10] D. A. Dikin, S. Stankovich, E. J. Zimney, R. D. Piner, G. H. B. Dommett, G. Evmenenko, S. T. Nguyen and R. S. Ruoff, *Nature*, 2007, **448**, 457–460.

[11] S. Stankovich, D. A. Dikin, G. H. B. Dommett, K. M. Kohlhaas, E. J. Zimney, E. A. Stach, R. D. Piner, S. T. Nguyen and R. S. Ruoff, *Nature*, 2006, **442**, 282–286.

[12] X. Huang, Z. Y. Yin, S. X. Qi, X. Y. Wu, Q. Y. He, Q. C. Zhang, Q. Y. Yan, F. Boey and H. Zhang, *Small*, 2011, **7**, 1876-1902.

[13] S. Stankovich, D. A. Dikin, R. D. Piner, K. M. Kohlhaas, A. Kleinhammes and Y. Jia, *Carbon*, 2007, **45**, 1558–1565.

[14] Y. X. Xu, W. J. Hong, H. Bai, C. Li and G. Q. Shi, *Carbon*, 2009, **47**, 3538-3543.

[15] Y. W. Zhu, S. Murali, W. W. Cai, X. S. Li, J. W. Suk, J. R. Potts, R. S. Ruoff, *Advanced materials*, 2010, **22**, 3906-3924.

[16] J. H. Wu, Q. W. Tang, H. Sun, J. M. Lin, H. Y. Ao, M. L. Huang and Y. Huang, *Langmuir*, 2008, **24**, 4800–4805.

[17] W. H. Kai, Y. Hirota, L. Hua and Y. Inoue, *J Appl Polym Sci*, 2008, **107**, 1395–400.

[18] G, Scalia, J, P. F. Lagerwall, S. Schymura, M. Haluska, F. Giesselmann and S. Roth, *phys. stat. sol. (b)*, 2007, **244**, 4212-4217.

[19] W. Q. Jiang, B. Yu, W. M. Liu and J. C. Hao, *Langmuir*, 2007, **23**, 8549-8553.

[20] D. Michael, D. Lynch and L. Patrick, *Nano Letters*, 2002, **2**, 1197-1201.

[21] G. Scalia, C. von Bühler, C. Hägele, S. Roth, F. Giesselmann and J. Lagerwall, *Soft Matter*, 2008, **4**, 570–576.

[22] F. Tardani, C. Pucci and C. La Mesa, *Soft Matter,* 2014, **10**, 1024-1031.

[23] F. Tardani and C. La Mesa, *J. Phys. Chem. C,* 2011, **115**, 9424 –9431.

[24] F. Tardani, L. Gentile, G. A. Ranieri and C. La Mesa, *J. Phys. Chem. C*, 2013, **117**, 8556 − 8562.

[25] S. E. Moulton, M. Maugey, P. Poulin and G. G. Wallace, *J. Phys. Chem. C*, 2012, **116,** 9888-9894.

[26] V. Weiss, R. Thiruvengadathan and O. Regev, *Langmuir,* 2006, **22**, 854–856.

[27] X. Xin, H. Li, S. A. Wieczorek, T. Szymborski, E. Kalwarczyk, N. Ziębacz, E. Gorecka, D. Pociecha and R. Holyst, *Langmuir,* 2010, **26,** 3562–3568.

[28] X. Xin, M. Pietraszkiewicz, O. Pietraszkiewicz, O. Chernyayeva, T. Kalwarczyk, E. Gorecka, D. Pociecha, H. Li and R. Hołyst, *Carbon*, 2012, **50,** 436–443.

[29] L. Wang , X. Xin, K. Guo, M. Z. Yang, X. Ma, J. Yuan, J. L. Shen and S. L. Yuan, *Phys. Chem. Chem. Phys.*, 2014, **16,** 14771–14780.

[30] D. J. Mitchell, G. J. T. Tiddy, L. Waring, T. Bostock and M. P. McDonald, J. Chem. Soc. Faraday Trans. 1, 1983, 79, 975-1000.

[31] D. Li, M. B. Muller, S. Gilje, R. B. Kaner and G. G. Wallace, *Nature Nanotechnol.,* 2008, **3**, 101-105.

[32] X. Xin, H. Li, S. A. Wieczorek, T. Szymborski, E. Kalwarczyk, N. Ziębacz, E. Gorecka, D. Pociecha and R. Holyst, *Langmuir,* 2010, **26,** 8821–8828.

[33] H. S. Jang, T. H. Kim, C. Do, M. J. Lee and S. M. Choi, *Soft Matter*, 2013, **9**, 3050-3056.

[34] P. Terech, S. Dourdain, U. Maitra and S. Bhat, *J. Phys. Chem. B*, 2009, **113**, 4619-4630.

[35] S. S. Song, L. Feng, A. X. Song and J. C. Hao, *J. Phys. Chem. B*, 2012, **116**, 12850-12856.

[36] A. Pal, H. Basit, S. Sen, V. Aswal and S. Bhattacharya, *J. Mater. Chem.*, 2009, **19**, 4325–4334.

[37] J. C. Fan, Z.X. Shi, M. Lian, H. Li and J. Yin, *J. Mater. Chem. A*, 2013, **1**, 7433-7443.